

COMPARISON OF ELECTRON EMISSION IN LINEARLY AND CIRCULARLY POLARIZED GAUSSIAN FIELDS

© 2024 A. V. Borovskiy^a, A. L. Galkin^{b*}

^a Baikal State University 664003, Irkutsk, Russia

^b Prokhorov General Physics Institute, Russian Academy of Sciences, 119991, Moscow, Russia

*e-mail: galkin@kapella.gpi.ru

Received September 11, 2023

Revised January 23, 2024

Accepted January 23, 2024

Abstract. A comparative analysis of electromagnetic emission by an electron in Gaussian fields of linear and circular polarization was carried out. For a short laser pulse, local (power in solid angle and power) and integral (energy emitted from the trajectory) characteristics of emission are determined. It is shown that the previously discovered law of growth of the emitted peak angular power in a linearly polarized field also extends to the case of a circularly polarized field with a decrease in the numerical coefficient by a factor of 2 due to a decrease in the field amplitude by a factor of $\sqrt{2}$. During backscattering in both considered cases of linear and circular polarization, the emission characteristics have a power-law increase with indices 6 (peak power per solid angle) and 4 (power, radiated energy) in terms of the initial electron energy and significantly exceed the values of the radiation characteristics from symmetric trajectories.

An estimate of the radiated angular power in the direction of the motion speed is obtained.

Keywords: *UV and soft-X-ray generation, emitted electromagnetic field, radiation reaction force, residual electron oscillation energy, integral emission energy*

DOI: 10.31857/S004445102406e026

1. INTRODUCTION

A charged particle experiences maximum impact from the electromagnetic field in the vicinity of the laser pulse focus. As a result, the electron radiation spectrum can reach X-ray and gamma ranges [1]. The study of radiation generation has both applied and fundamental significance. Radiation sources with prediction of peak intensity values and radiation power distribution are of interest in biomedicine and atomic physics [2,3]. Applied task formulations are based on the initial position of a "stationary" electron directly in the laser pulse focus, which leads to radiation in the form of classical Thomson scattering with "forward-backward" symmetry. The radiation of an electron that acquires kinetic energy due to interaction with the field is interpreted as nonlinear Thomson scattering. In the case of electron counter-propagation relative to the laser pulse, electron radiation also fits into the scheme of nonlinear Thomson scattering.

From a fundamental perspective, obtaining maximum radiation characteristics is of interest, as well as establishing radiation features in connection with the possibility of radiation-dominant regime emergence [4–5]. A notable contribution of radiation friction is noted in works [6–8].

Various aspects of nonlinear Thomson scattering are considered in works [9–11]. The development of methods for calculating radiation power, alternative to the relativistic Larmor formula [12], is relevant. Thus, in work [13], a methodology for constructing electron radiation diagrams is proposed, which also allows determining the directionally integrated radiation power. A power-law growth with an exponent of 6 for the angular power of backscattering in a linearly polarized laser field with respect to the initial electron kinetic energy was discovered [14].

The aim of this work is a comparative analysis of electron radiation in laser fields of linear and circular polarization.

2. MODELS OF FOCUSED LASER FIELD

When choosing a focused laser field model, one is usually guided by the criterion of accuracy in correspondence with Maxwell's equations. The second important criterion is the consistency of theory with experiment. The complexity of model implementation should also be considered. Let's evaluate the models according to these criteria.

The model of transverse fields with a flat phase front and inhomogeneous transverse distribution does not satisfy Maxwell's equations [15]. It was used, for example, in works [6–8]. In general, it does not describe the axially symmetric ejection of ionization electrons from the interaction region with a linearly polarized laser field observed in experiments. It describes ejection along the polarization direction, which according to existing understanding is not important for the problems solved in works [6–8].

The model of Gaussian beams with transverse-longitudinal field components, due to accounting for the phase front tilt, is a solution to the parabolic equation — an approximation of the wave equation — a direct consequence of Maxwell's equations in vacuum, i.e., it is an approximate solution to Maxwell's equations [18]. There are many solutions in the form of Gauss–Laguerre fields. The fundamental Gauss–Laguerre mode has an exponentially decreasing transverse inhomogeneity from the axis. This field distribution satisfies the criterion of axial symmetry for electron ejection from the interaction region. The applicability conditions for this approximation are as follows:

$$\varepsilon = \frac{1}{kp_0}, \quad d = \frac{1}{kL}, \quad \varepsilon^2 \ll 1, \quad \delta \ll 1.$$

Here ρ_0 is the transverse waist size of the laser pulse at half-height in the focal plane, L is the longitudinal size of the laser pulse, k is the wave number of laser radiation. The coefficient ε^2 appears in the wave equation for the complex amplitude of the vector potential. Note that both conditions are obtained when applying the method of variable separation to the wave equation and are less burdensome than in other works. The first condition limits the focal spot size from below. The second condition limits the envelope application since $L = c\tau$, τ is the pulse duration, c is the speed of light.

2.1. Field Models Based on Exact Solution of Maxwell's Equations

Maxwell's equations in vacuum reduce to the wave equation for vector potential, which should be solved with boundary conditions on the focusing lens surface. The solution of the linear wave equation with boundary conditions can be obtained through variable separation methods, reduction to Kirchhoff's integral, and Fourier–Laplace transformation. The paper [19] presents some exact solutions of Maxwell's equations describing time-stationary focused laser pulses. In particular, the electric-type laser pulse with transverse electric field and transverse-longitudinal magnetic field differs from the fundamental Gauss–Laguerre mode. As it approaches the diffraction limit, the solution transitions into a Gaussian beam-type field distribution, representing a complex combination of Gauss–Laguerre modes. The model was applied [20] to interpret experiments with asymmetric electron acceleration [21]. We should also note the construction of sharply focused fields using the generalized Kirchhoff integral [18].

Thus, when considering laser fields with focusing not reaching the diffraction limit, the most suitable are the fields of the fundamental Gauss–Laguerre mode — Gaussian beam. In this article $kp_0 = 26.7$, $kL = 10$. Therefore, the Gaussian beam approximation is adequate. In terms of model implementation complexity, the computation volume in this work exceeds that of [14] by an order of magnitude. Increasing the pulse duration would lead to an inefficient increase in computation volume at distances far from the focus.

The vector potential of a Gaussian beam laser field propagating along the axis in the vicinity of the focus can be represented as

$$A = A_0 \cos \sigma \exp \left(-\frac{1}{2} \rho^2 \cos^2 \sigma \right) \times \left(e_x \sqrt{\frac{1+\alpha}{2}} \cos \varphi_{ph} + e_y \sqrt{\frac{1-\alpha}{2}} \sin \varphi_{ph} \right), \quad (1)$$

where A_0 and φ_{ph} — are amplitude and phase,

$$\varphi_{ph} = \omega t - kz + \sigma - \frac{1}{4} \rho^2 \sin 2\sigma,$$

$$\cos^2 \sigma = \frac{1}{1 + (z / z_R)^2}, \quad (2)$$

$$z_R = k \rho_0^2, \quad \rho = r / \rho_0,$$

r is the transverse coordinate, e_x, e_y are unit vectors. Linear polarization along x and y corresponds to values $\alpha = 1$ and $\alpha = -1$, circular — $\alpha = 0$, for other values in the interval $(-1, 1)$ the polarization is elliptical. The peak intensity (time-averaged Poynting vector magnitude) is identical and is defined through the relativistic intensity

$$I_0 = \frac{c}{8\pi} (A_0 k)^2 = \mu I_R,$$

$$I_R = \frac{m^2 c^5 \pi}{2 e^2 \lambda^2},$$

where m and e are the electron rest mass and charge. If μ , is given, then A_0 is determined. Fields in the general case of elliptical polarization are determined by components $(E_x, E_y, \delta E_z, H_x, H_y, \delta H_z)$, longitudinal components $\delta E_z, \delta H_z \approx \varepsilon = 1 / k \rho_0$, (paper [22] considers expressions for fields with higher orders ε , but the advantage of such expansion is not discussed). As follows from expression (1), the amplitude of the main (transverse) field in the case of circular polarization ($\alpha = 0$) is $\sqrt{2}$ times smaller than the amplitude of linear polarization ($\alpha = \pm 1$), and the maximum amplitude of elliptical polarization has an intermediate value, so that for the numerical factors of these amplitudes, the inequalities

$$\frac{1}{\sqrt{2}} \leq \sqrt{\frac{1}{2} + \frac{|\alpha|}{2}} \leq 1.$$

hold. When transitioning from a Gaussian beam to a pulse also with a Gaussian time distribution, the field description should include a temporal envelope as a multiplier

$$\exp \left(- \left(\frac{t - (z - z_d) / c}{2\tau} \right)^2 \right),$$

where τ is the pulse duration at half intensity, z_d is the initial distance from the temporal envelope maximum to the focal plane.

3. ELECTRON MOTION TRAJECTORIES IN GAUSSIAN FIELDS OF DIFFERENT POLARIZATION

Solutions of the Lorentz equation with initial conditions and the complete set of field components $(E_x, E_y, \delta E_z, H_x, H_y, \delta H_z)$,

$$m \frac{d}{dt} \left(\frac{\frac{dr}{dt}}{\sqrt{1 - \left(\frac{v}{c} \right)^2}} \right) = -eE - \frac{e}{c} \frac{dr}{dt} \times H, \quad (3)$$

$$r(0) = r_0, \quad v(0) = v_0,$$

allow determining the electron motion trajectory, as well as instantaneous values of velocity components v and acceleration v' .

The standard problem (3) of three nonlinear second-order differential equations is numerically solved using Wolfram Mathematica package, but requires decomposition of relativistic nonlinearity (it is necessary to expand all derivatives component-wise and reduce to normal form with isolation of higher derivatives, which explains the notation (3)). Testing is performed by constructing symmetric trajectories: the electron initially rests on the pulse axis before the focus and after interaction with the pulse stops at the same distance beyond the focus. Selection of initial conditions ensures compensation of the dynamic impact when the field is turned on. Calculation of the motion of an initially resting electron, displaced from the axis, in the field of a Gaussian pulse of the fundamental mode leads to symmetric ejection from the interaction region.

A short pulse $\tau c / \lambda = 1.5$, corresponding to a duration of 3.5 fs is considered. Figure 1 shows symmetric trajectories of electron motion in fields with parameters $\rho_0 = 26.7$, $\tau c / \lambda = 1.5$, $\mu = 5$ (waist size, temporal envelope length in oscillation periods, and peak intensity μ relative to relativistic) of different polarization $\alpha = 0(a), 1(b), -1(c)$. Initial data for problem (3):

$$x_0 / \lambda = 0, y_0 / \lambda = 0, z_0 / \lambda = -1.2,$$

$$v_{0x} / c = 10^{-18}, v_{0y} / c = 5 \cdot 10^{-10}, v_{0z} / c = 10^{-18}.$$

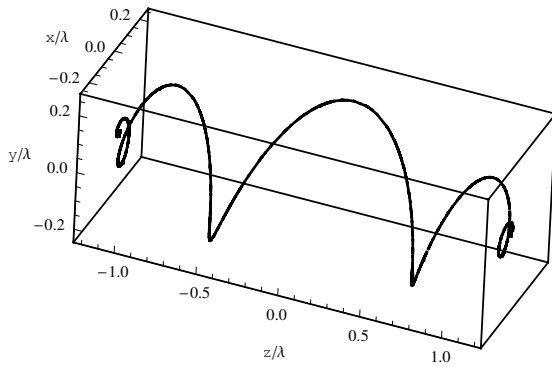
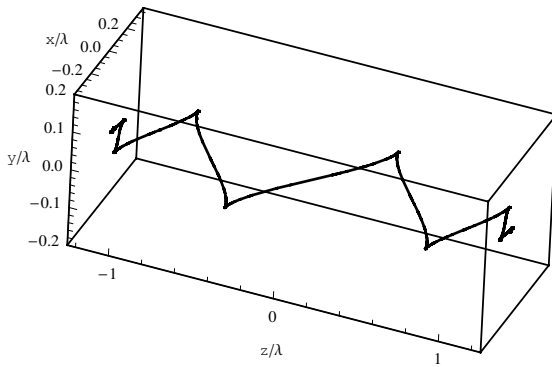
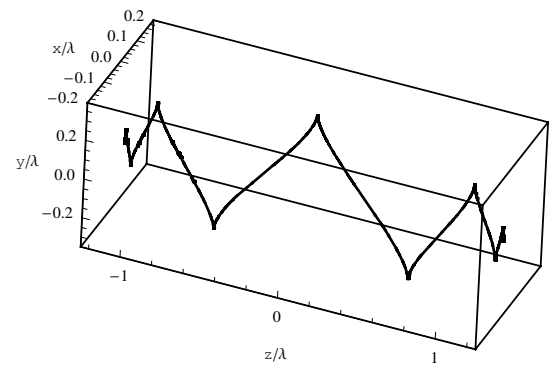
*a**b**c*

Fig. 1. Symmetric electron trajectories at $\mu = 5$, $\tau c / \lambda = 1.5$, $\alpha = 0$ (a), 1 (b), -1 (c)

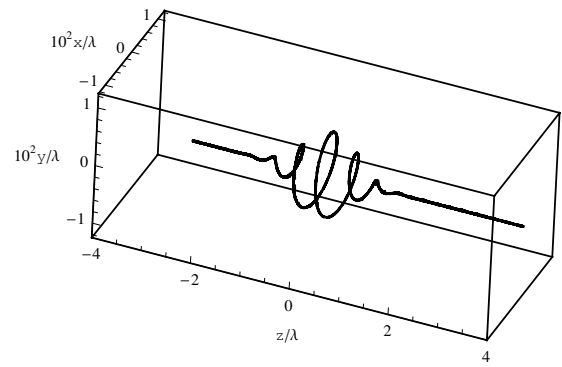
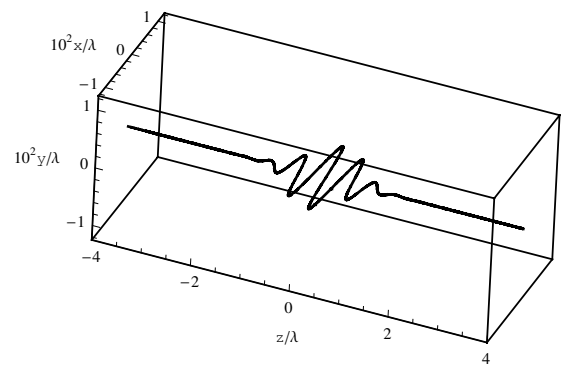
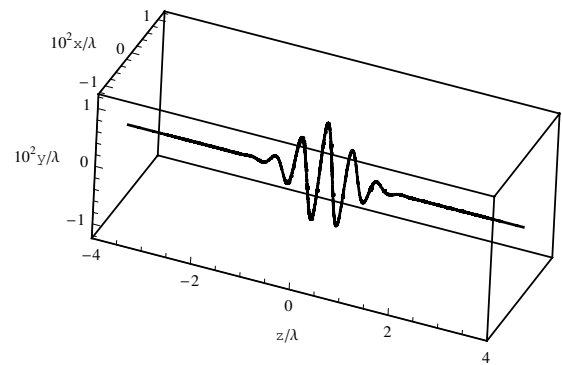
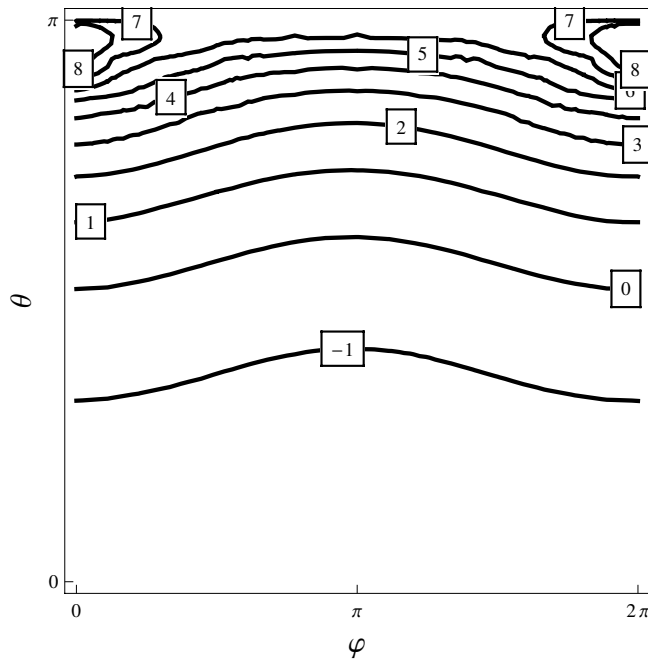
*a**b**c*

Fig. 2. Trajectories of electron motion with initial kinetic energy $p = 20$ towards the laser pulse with parameters $k_{p0} = 26.7$, $\tau c / \lambda = 1.5$, $\mu = 5$ of different polarization $\alpha = 0$ (a), 1 (b), -1 (c)

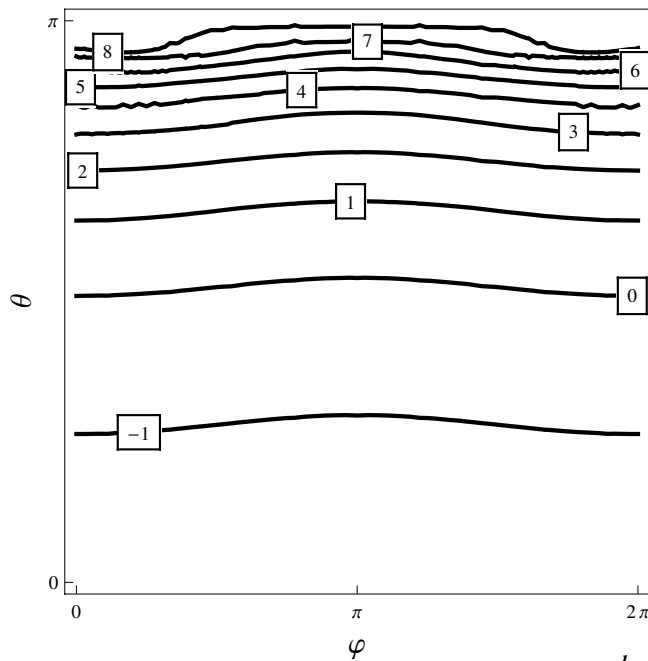
Trajectories $\alpha = 1$ (Fig. 1b), $\alpha = -1$ (Fig. 1c) do not coincide when rotated around axis z by angle $\pi / 2$, as the acting fields (1) are phase-shifted. For an electron moving towards the laser pulse, the initial velocity is related to the initial kinetic energy

$$\frac{W_{k_0}}{mc^2} = \frac{1}{\sqrt{1 - (v_{0z} / c)^2}} - 1 = p.$$

Since symmetric trajectories, besides the test value, describe the maximum radiation energy compared to all trajectories of an initially resting electron (not only on the axis) at fixed laser pulse parameters, we will further assume that motion along symmetric trajectories corresponds to the case $p = 0$. For $p > 0$ we assume that the electron passes near the focus at the moment of the temporal envelope maximum. This corresponds to a change in



a



b

Fig. 3. Level lines $\lg[I_1^{-1} dI / d\Omega(\varphi, \theta)]$ of electron radiation with initial kinetic energy $p = 10$ towards the laser pulse with parameters $k\rho_0 = 26.7$, $\tau c / \lambda = 1.5$, $\mu = 5$ of different polarization $\alpha = 0$ (a), 1 (b)

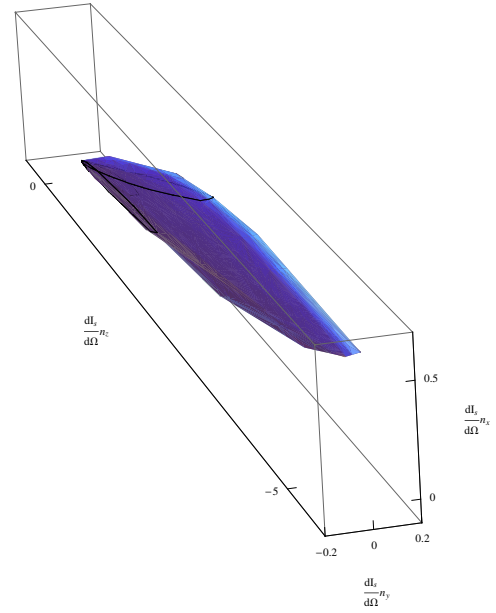


Fig. 4. Radiation pattern of the electron, built according to the distribution in Fig Figure 3a ($p = 10$, $\alpha = 0$)

initial conditions $z_0 = v_{0z}(p)z_d / c$, $v_{0z} = v_{0z}(p)$ — the magnitude of the counter velocity determined by p . Fig. 2 shows electron motion trajectories in fields with parameters $k\rho_0 = 26.7$, $\tau c / \lambda = 1.5$, $\mu = 5$ of different polarization $\alpha = 0, 1, -1$ and with initial kinetic energy $p = 20$ (electron moves in the direction of decreasing coordinate z). Since $z_d = 6\lambda$, and $v_{0z}(20) / c = 0.998866$, initial conditions $z_0 / \lambda = 6$, $v_{0z} / c = -0.998866$, others as for symmetric trajectories.

4. ELECTRON RADIATION IN GAUSSIAN FIELDS

Electron motion occurs under the action of the Lorentz force, while the electron emits electromagnetic pulses. In the radiation model based on Lienard-Wiechert potentials, the electron emits field

$$\mathbf{E}_{rad} = e \frac{1 - v^2 / c^2}{(R - \mathbf{R} \cdot \mathbf{v} / c)^3} \left(\mathbf{R} - \frac{\mathbf{v}}{c} R \right) + \frac{e}{c^2 (R - \mathbf{R} \cdot \mathbf{v} / c)^3} [\mathbf{R} \times \left[\left(\mathbf{R} - \frac{\mathbf{v}}{c} R \right) \times \mathbf{v}' \right]], \quad (4)$$

$$t_r + \frac{R(t_r)}{c} = t.$$

For $\mathbf{R} = R\mathbf{n}$, $R \sim 10^4 \lambda$ we have

$$\mathbf{E}_{rad} = e \frac{1 - v^2 / c^2}{R^2 (1 - \mathbf{n} \cdot \mathbf{v} / c)^3} \left(\mathbf{n} - \frac{\mathbf{v}}{c} \right) + \frac{e}{c^2 R (1 - \mathbf{n} \cdot \mathbf{v} / c)^3} \left[\left(\mathbf{n} - \frac{\mathbf{v}}{c} \right) \times \mathbf{v}' \right]. \quad (5)$$

The distribution of radiation power over the solid angle Ω in the direction \mathbf{n} (hereinafter briefly referred to as intensity),

$$\mathbf{n} = (\sin \theta \cos \varphi, \sin \theta \sin \varphi, \cos \theta),$$

focus has coordinates $(0, 0, 0)$, θ — azimuthal angle from the focus relative to the axis z , φ — polar angle in the focal plane xy , is determined by the second (radiative) term in (4):

$$\frac{dI}{d\Omega} = \frac{1}{4\pi} \frac{e^2}{c^3 (1 - \mathbf{n} \cdot \mathbf{v} / c)^6} \left| \mathbf{n} \times \left[\left(\mathbf{n} - \frac{\mathbf{v}}{c} \right) \times \mathbf{v}' \right] \right|^2. \quad (6)$$

To construct the radiation directivity pattern in the Lienard–Wiechert model, it is necessary to calculate the distribution $dI / d\Omega(\varphi, \theta)$ and construct the surface $\mathbf{n} dI / d\Omega$. Integration of expression (6) over the solid angle gives the power radiated by the electron at a given moment of time. Normalization of radiation patterns $\mathbf{n} dI / d\Omega$ in the Lienard–Wiechert model is performed by the value

$$I_1 = \frac{2}{3} \frac{e^2}{\lambda} \frac{1}{\lambda / c}.$$

Determination of the maximum value of radiated power into the solid angle, $dI / d\Omega$, consists in conducting optimization calculations. A methodology has been developed [23]; the task is non-standard; the program is implemented in Fortran. Fig. 3 shows the level lines of distributions $\lg \left[I_1^{-1} dI / d\Omega(\varphi, \theta) \right]$ of maximum-in-time radiation of the counter electron ($p = 10$) in the field of a laser pulse with parameters $k\rho_0 = 26.7$, $\tau c / \lambda = 1.5$, $\mu = 5$ for circular ($\alpha = 0$) and linear ($\alpha = 1$) polarizations. As follows from Fig. 3, in the case of linearly polarized field, backscattering occurs into a narrow cone in the vicinity of $\theta = \pi$ and is well described by expression

$$\frac{1}{I_1} \frac{dI}{d\Omega} \Big|_{\theta=\pi} \cong$$

$$\cong 6\pi\mu(p+1)^6 \left[1 + \sqrt{1 - \frac{1}{(p+1)^2}} \right]^4. \quad (7)$$

In the case of circular polarization, the radiation solid angle is inclined due to electron motion in a circle in the focal plane and is concentrated in the vicinity of $\theta = 0.95\pi$. The electron radiation directivity pattern for this case $10^{-8} / I_1 (\mathbf{n} dI / d\Omega)$

is shown in Fig. 4. Maximum angular power is the maximum longitudinal size of the pattern; main radiation goes into a cone; the cone is inclined.

To estimate the maximum radiation intensity without optimization, the following approach is proposed. The denominators of expression (4) are maximum at $\mathbf{n} \parallel \mathbf{v}$, i.e., we can set $\mathbf{n} = \mathbf{v} / v$, then

$$\begin{aligned} & \left[\mathbf{n} \times \left[\left(\mathbf{n} - \frac{\mathbf{v}}{c} \right) \times \mathbf{v}' \right] \right] = \\ & = \left(\left(\mathbf{n} - \frac{\mathbf{v}}{c} \right) (\mathbf{n} \cdot \mathbf{v}') - \mathbf{v}' \left(1 - \frac{\mathbf{n} \cdot \mathbf{v}}{c} \right) \right) \cong \\ & \cong \left(\left(\frac{\mathbf{v}}{v} - \frac{\mathbf{v}}{c} \right) \left(\frac{\mathbf{v}}{v} \cdot \mathbf{v}' \right) - \mathbf{v}' \left(1 - \frac{v}{c} \right) \right) = \\ & = \left(1 - \frac{v}{c} \right) \left(\frac{\mathbf{v}}{v^2} (\mathbf{v} \cdot \mathbf{v}') - \mathbf{v}' \right), \\ & \left[\mathbf{n} \times \left[\left(\mathbf{n} - \frac{\mathbf{v}}{c} \right) \times \mathbf{v}' \right] \right]^2 \cong \\ & \cong \left(1 - \frac{v}{c} \right)^2 \left(\frac{(\mathbf{v} \cdot \mathbf{v}')^2}{v^2} + (\mathbf{v}')^2 - 2 \frac{(\mathbf{v} \cdot \mathbf{v}')^2}{v^2} \right) = \\ & = \left(1 - \frac{v}{c} \right)^2 \left((\mathbf{v}')^2 - \frac{(\mathbf{v} \cdot \mathbf{v}')^2}{v^2} \right), \\ & \max \left[\frac{dI}{d\Omega} \right] = \frac{c E_{rad}^2}{4\pi} R_0^2 = \\ & = \frac{c}{4\pi} R_0^2 \frac{e^2}{c^4 R_0^2 (1 - v / c)^6} \left(1 - \frac{v}{c} \right)^2 (\mathbf{v}')^2 \sin^2(\angle \mathbf{v} \mathbf{v}') = \\ & = \frac{e^2 (\mathbf{v}')^2 \sin^2(\angle \mathbf{v} \mathbf{v}')}{4\pi c^3 (1 - v / c)^4}. \end{aligned} \quad (8)$$

To characterize the velocity of motion, we use kinetic energy W_k / mc^2 . The time course of kinetic energy and acceleration modulus over time is shown in Fig. 5.

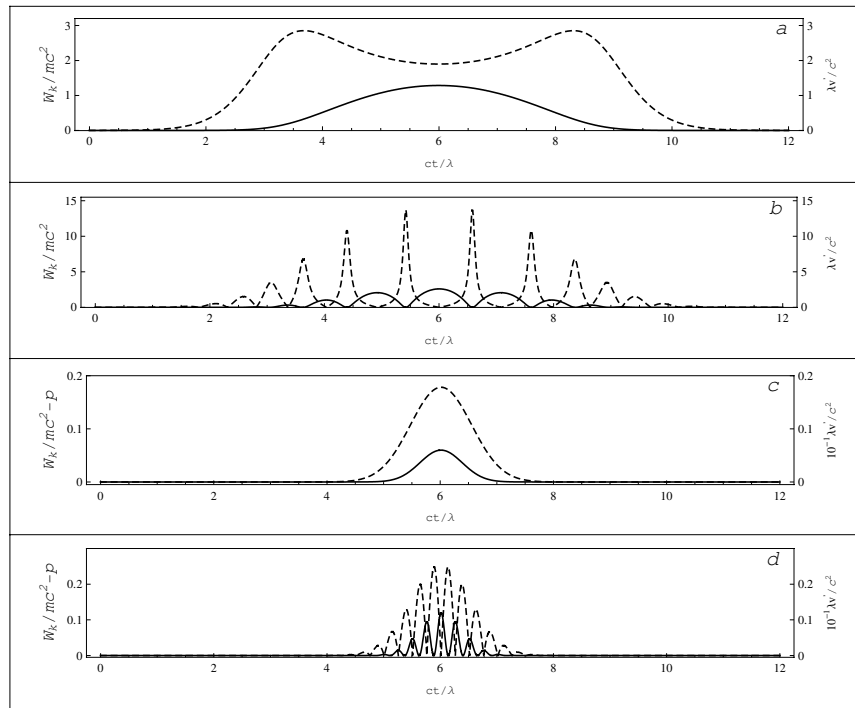


Fig. 5. Time course of kinetic energy W_k / mc^2 (solid curve) and acceleration modulus $|\mathbf{v}'|\lambda/c^2$ (dashed curve) of the electron moving along trajectories: $\alpha = 0, p = 0$ (a); $\alpha = 1, p = 0$ (b); $\alpha = 0, p = 10$ (c); $\alpha = 1, p = 10$ (d)

5. CALCULATION OF ELECTRON RADIATION CHARACTERISTICS IN GAUSSIAN FIELDS

The following characteristics are of interest.

1. Maximum power per solid angle, $\max[dI/d\Omega]$ normalized to I_1 .
2. Radiation power

$$I = \int \frac{dI}{d\Omega} d\Omega$$

also normalized to I_1 .

3. Radiated energy from the trajectory of motion

$$E = \int I dt$$

normalized to

$$E_1 = \frac{2}{3} \frac{e^2}{\lambda},$$

where for $\lambda = 800$ nm

$$E_1 \frac{1}{mc^2} = \frac{2}{3} \frac{e^2}{\lambda} \frac{1}{mc^2} \approx 2.35 \cdot 10^{-9}.$$

Figure 6a shows the temporal progression of electron radiation power during motion along symmetric trajectories in Fig. 1 for $\alpha = 0, 1, -1$. Radiation bursts with linear polarization sometimes exceed radiation power values with circular polarization, which is associated with higher acceleration values. The energy radiated from trajectories (integral of power over time) at $p = 0$, equals $E/E_1 = 1.83 \cdot 10^3$ ($\alpha = 0$); $1.01 \cdot 10^3$ ($\alpha = 1$); $1.02 \cdot 10^3$ ($\alpha = -1$).

In Fig. 6b shows the temporal progression of electron radiation power with initial kinetic energy $p = 20$ during motion along trajectories in Fig. 2 for ($\alpha = 0, 1, -1$). The energy radiated from trajectories at $p = 20$ increases by orders of magnitude and equalizes across polarizations: $E/E_1 = 1.03 \cdot 10^8$ ($\alpha = 0$); $1.08 \cdot 10^8$ ($\alpha = 1$); $1.10 \cdot 10^8$ ($\alpha = -1$).

Summary information on the dependence of radiation characteristics on initial kinetic energy is presented in Fig. 7. Calculated values are shown as points in black ($\alpha = 0$), blue ($\alpha = 1$) and red ($\alpha = -1$) colors. The upper curve 1 (a straight line in logarithmic scale) is the dependence (7); according to work [14], this curve contains the values of maximum angular radiation power in a linear

polarization field, $\alpha = \pm 1$. Curve 2 is a dependence of type (7) with half the coefficient; this curve contains the values of maximum angular radiation power in a circular polarization field, $\alpha = 0$. On the approximation curve 3

$$\frac{I_{\max}}{I_1} \cong 64\pi\mu(p+1)^4$$

lie the values of maximum radiation power in a linear polarization field, $\alpha = \pm 1$. On the approximation curve 4

$$\frac{I_{\max}}{I_1} \cong 32\pi\mu(p+1)^4$$

lie the values of maximum radiation power in a circular polarization field, $\alpha = 0$.

The energy dependencies E/E_1 , radiated from trajectories both in linear and circular polarization, $\alpha = 0, \pm 1$, in the considered logarithmic scale and with the used non-dimensionalization, coincide with high accuracy with the dependence I_{\max}/I_1 for $\alpha = 0$ and lie on the approximating curve 4.

6. DISCUSSION OF RESULTS

According to estimation (8), the intensity maximum can be achieved at the maximum of velocity and acceleration moduli, while $\sin^2(\mathbf{v}', \mathbf{v}) \approx 1$. The time coincidence of maxima occurs for $\alpha = 0, p > 0$ (Fig. 4c), in this case, approximation (8) works well. In the case of $\alpha = \pm 1, p = 0$ (Fig. 4b), there is a time separation of velocity and acceleration moduli maxima [14]. In the case of $\alpha = \pm 1, p > 0$ (Fig. 4d), backscattering occurs in the direction opposite to the z ($\theta = \pi$), axis, at the moment when the maximum of the modulus v_y and $v_z = v_{0z}$ is reached; under these assumptions, estimation (7) was obtained [14]. The agreement of calculations for circular polarization $\alpha = 0, p > 0$ with the approximating curve (with a coefficient reduced by 2 due to field amplitude reduction by $\sqrt{2}$ times) extends the limits of analytical applicability. At the direction of maximum intensity radiation has an inclination due to electron motion in a circle in the focal plane (see Fig. 3a and Fig. 4). Also, the dependencies of radiation power maxima differ by a factor of two for linear and circular polarization (dependencies 3, 4 in Fig. 7).

Overall, the scattering process responds to instantaneous values of field intensity (Poynting vector modulus) without averaging over the wave period, therefore, the generalization of expression (7) for elliptically polarized field consists in adding the factor $1/2 + |\alpha|/2$. Thus, for an elliptically polarized field, an intermediate position should be expected between dependencies 1, 2 for maximum power into solid angle and 3, 4 for maximum radiation power with a change relative to characteristics at linear polarization by $1/2 + |\alpha|/2$ times.

In the field of linear polarization, $\alpha = \pm 1, p = 0$, radiation with sharp piecewise-linear symmetric trajectory (Fig. 1b, c) transforms into a smoothed temporal profile of radiation power (Fig. 3a) and, conversely, radiation from a smoothed trajectory $\alpha = \pm 1, p > 0$ at high values p (Fig. 2b, c) transforms into a sharp temporal profile of radiation power (Fig. 3b). On symmetric trajectories at $\alpha = 0, p = 0$ longitudinal and transverse velocity components are comparable, and at the moment of reaching the maximum velocity modulus lead to higher values of radiation power and energy emitted from the trajectory compared to the case $\alpha = 1, p = 0$, where there is temporal separation of velocity and acceleration moduli maxima. At large values, the difference in field amplitudes for $\alpha = \pm 1, p > 0$ and $\alpha = 0, p > 0$ leads to a twofold difference in maximum power values. Due to quasi-linear change in radiation power for $\alpha = \pm 1, p > 0$ during the wave period, the radiation energy from trajectories coincides with the emitted energy in the circular polarization field, $\alpha = 0, p > 0$, and normalization to E_1 leads to the coincidence of dependencies 4 in Fig. 7. This coincidence is accidental, since only the energy emitted from the trajectory increases with the laser pulse duration. The energy emitted from the trajectory increases as a power law, as $(p+1)^4$, with increasing initial electron kinetic energy, reaching values of 0.132 MeV for $\lambda = 800$ nm in the considered range p and for the given pulse duration. Significantly higher values of emitted energy from the symmetric trajectory ($p = 0$) in the circular polarization field compared to radiation in the linear polarization field and the equalization of emitted energy by polarization at $p = 20$ can be explained by the decrease in electron orbit radius with increasing p . The question of

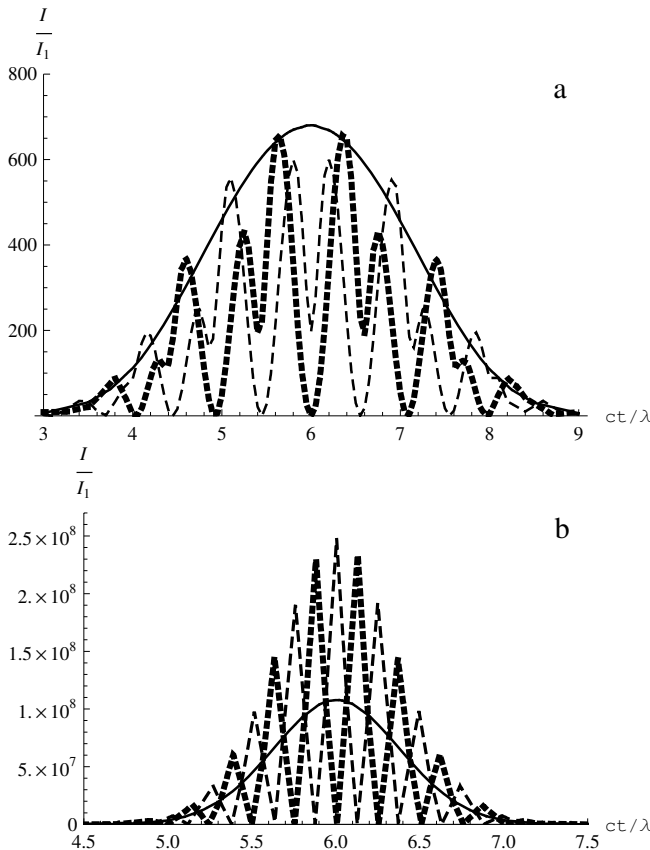


Fig. 6. Time evolution of electron radiation power during motion: *a* – along symmetric trajectories Fig. 1; *b* – with initial kinetic energy $p = 20$ along trajectories Fig. 2; $\alpha = 0$ (solid curves), $\alpha = 1$ (dashed curves), $\alpha = -1$ (dotted curves)

studying the dependence of electron orbit radius in the focal plane on gaussian pulse parameters of circular polarization and on electron energy is interesting for separate consideration.

7. CONCLUSIONS

A comparative analysis of electron radiation in Gaussian fields of linear and circular polarizations has been conducted. An estimate of the radiated power into the solid angle in the direction of motion velocity was obtained. Local (power into solid angle and power) and integral (energy radiated from trajectory) radiation characteristics were determined. During backscattering in a circularly polarized field, the direction of maximum intensity radiation is inclined due to electron motion in a circle in the focal plane, but due to the small radius, this does not lead to a difference in energy radiated from the trajectory compared to the case of linearly polarized field, as for symmetric trajectories. It is shown that the peak intensity growth law discovered in work [14]

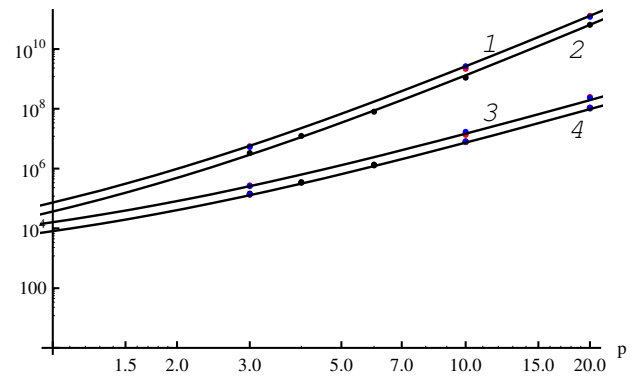


Fig. 7. Dependencies of radiation characteristics on initial kinetic energy p : maximum angular radiation power in linear polarization field $\alpha = \pm 1$ (curve 1); maximum angular radiation power in circular polarization field $\alpha = 0$ (curve 2); radiation power in linear polarization field $\alpha = \pm 1$ (curve 3); radiation power in circular polarization field $\alpha = 0$ and energy radiated from trajectories under linear and circular polarizations $\alpha = 0, \pm 1$ (curve 4)

for linear polarization field extends to the case of circular polarization field. The numerical coefficient decreases by 2 times due to the decrease in field amplitude by $\sqrt{2}$ times. During backscattering in both considered cases of linear and circular polarizations, the radiation power and radiated energy grow as $(p + 1)^4$ with respect to the initial electron energy and significantly exceed the values of radiation characteristics from symmetric trajectories.

ACKNOWLEDGMENTS

The authors thank M. V. Fedorov for pointing out the possibility of interpreting the results for elliptical polarization.

REFERENCES

1. A.L. Galkin, V.V. Korobkin, M. Yu. Romanovsky et al., Proc. of SPIE , 799319-1(2011).
2. A. Baltuška, Th. Udem, M. Uiberacker et al., Nature 421, 611 (2003).
3. K. Lee, Y.H. Cha, M.S. Shinet al., Phys. Rev. E 6, 7 026502 (2003).
4. S.V. Bulanov, T. Zh. Esirkepov, J. Koga et al., Plasma Physics Reports 30, 3, 196 (2004).
5. A.V. Bashinov, A.A. Gonoskov, A.V. Kim et al., Quantum Electronics. 43, No. 4, 291 (2013).
6. A. Di Piazza, K. Z. Hatsagortsyan, C.H. Keitel, Phys. Rev. Lett. 102, 254802 (2009).
7. A.L. Galkin JETP. 115, 2, 201 (2012).
8. C.N. Harvey, Phys. Rev. Accel. Beams 21, 114001 (2018).

9. Ju Gao, Phys. Rev. Lett. 93, 243001 (2004).
10. P.A. Golovinskii, E.A. Mikhin, JETP 113,545 (2011).
11. Yifan Chang, Zishuai Cai, Yuting Shen et al., Laser Physics 32, 035302(2022).
12. V.V. Lidskii, Bull. Lebedev Phys. Inst. 36,2, 31 (2009).
13. A.V. Borovskiy, A.L.Galkin, Laser Phys. 32, 084008 (2022).
14. A.V. Borovskiy, A.L. Galkin, Laser Phys. Lett. 20, 036002 (2023).
15. B. Quesnel, P. Mora, Phys. Rev. E 58, 3719 (1998).
16. S. Banerjee, S. Sepke, R. Shah et al., Phys. Rev. Lett. 95, 035004 (2005).
17. A.V. Borovskiy, A.L. Galkin, M.P. Kalashnikov. Phys. of Plasmas. 22, 043107 (2015).
18. A.V. Borovskiy, A.L. Galkin, Selected Problems of Laser Physics. Vacuum Electron Acceleration. Focusing by a Parabolic Mirror. Diffraction on an Edge as a Problem of Subwavelength Physics. Palmarium Academic Publishing, Saarbrücken, Deutschland (2016) 267p (in Russian).
19. V.S. Popov, V.D. Moore, N. B. Narozhny et al., JETP 122, 3, 539 (2016).
20. N.B. Narozhny, M.S. Fofanov, Phys. Letters A 295, 87 (2002).
21. G. Malka, E. Lefebvre, J.L. Miquel, Phys. Rev. Lett. 78, 3314 (1997).
22. Qingyu Yang, Yubo Wang, Yifei Cao et al., Laser Physics Lett.,20, No. 4, 045301(2023).
23. A.V.Borovskiy, A.L. Galkin, System Analysis & Mathematical Modeling 6, in print (2024).